Bioactive Materials 5 (2020) 102–109

Contents lists available at ScienceDirect

Bioactive Materials

journal homepage: http://www.keaipublishing.com/biomat

Photoluminescent biodegradable polyorganophosphazene: A promising scaffold material for *in vivo* application to promote bone regeneration

Yiqian Huang[a], Zhaohui Huang[a], Huanhuan Liu[b], Xu Zhang[b], Qing Cai[a,*], Xiaoping Yang[a]

[a] State Key Laboratory of Organic-Inorganic Composites, Beijing Laboratory of Biomedical Materials, Beijing University of Chemical Technology, Beijing, 100029, China
[b] Department of Endodontics, School and Hospital of Stomatology, Tianjin Medical University, Tianjin, 300070, China

ARTICLE INFO

Keywords:
Tissue regeneration
Biodegradation
Photoluminescent
Polyorganophosphazene

ABSTRACT

Tissue engineering scaffolds made of conventional aliphatic polyesters are inherently non-fluorescent, which results in their *in vivo* degradation hard to be visualized. Photoluminescent biodegradable polyorganophosphazenes (PPOPs) are synthesized by introducing fluorophores onto the polyphosphazene backbone via nucleophilic substitution reaction. In this study, a fluorophore (termed as TPCA), derived from citric acid and 2-aminoethanethiol, was co-substituted with alanine ethyl ester onto the polyphosphazene backbone to obtain a photoluminescent biodegradable POPP (termed as PTA). The scaffolds made of PTA demonstrated non-cytotoxicity and cell affinity, particularly, capacity in promoting osteogenic differentiation of bone marrow mesenchymal stromal cells (BMSCs). *In vivo* evaluations using the rat calvarial defect model confirmed its strong potential in enhancing osteogenesis, more importantly, the *in vivo* degradation of the PTA scaffold could be monitored via its fluorescence intensity alongside implantation time.

1. Introduction

In the field of tissue engineering, the important roles of biodegradable scaffolds have been well-known, that their high porosity and proper morphology should endow favorable micro-environments for cell attachment, migration, proliferation and differentiation, and finally tissue regeneration [1]. Scaffolding materials are among the indispensable requirements to facilitate the clinical application of tissue engineering strategy [2–4]. Aliphatic polyesters such as polylactide (PLA), polyglycolide (PGA), polycaprolactone (PCL) and their copolymers are the most widely used biodegradable biomaterials in fabricating scaffolds with different designs [5–8]. When these materials are implanted *in vivo*, however, they are invisible because these conventional aliphatic polyesters lack functional groups that can be visualized using techniques like magnetic resonance imaging (MRI) or fluorescence imaging. Thus, it is difficult to reveal their degradation *in-situ* alongside new tissue formation [9,10]. Pushed by this concern, diverse attempts have been made to develop biodegradable biomaterials with bio-imaging potentials to achieve the goal.

Among the available bio-imaging systems, such as aggregation-induced emission (AIE) [11,12], photoacoustics (PA) [13,14], MRI [15,16] and photoluminescence excitation (PLE) [17], PLE is considered as a comparatively convenient and simple way to monitor the *in vivo* degradation of implanted materials [18]. The aforementioned aliphatic polyesters, however, additional modifications are necessary to endow them with photoluminescent performance because they are not inherently photoluminescent [19]. In reports, quantum dots (Qdots) like CdSe were incorporated for bio-imaging, which were not detrimental to cells within short time, however, they turned to be cytotoxic in the long period as the free Cd^{2+} ion being released [20]. Though the high fluorescent intensities of Qdots can satisfy the bio-imaging requirements for implantation, the potential toxicity from the heavy metal cores of Qdots are actually not welcomed for *in vivo* applications, which might cause biocompatibility concerns [21]. In our previous study, a fluorescent perylenediimide-cored dendritic star macromolecule was blended into poly(L-lactide) (PLLA) and poly(lactide-co-glycolide) (PLGA) to visualize their *in vivo* degradation [22]. Though the results were promising, a concern alongside the polymer degradation was the gradual release of the incorporated fluorescent component, which might provide misleading results. Yang et al. developed a series of photoluminescent polyesters as alternatives for lactide-based polyesters by condensation polymerization, in which, 1,8-octylene glycol, citric acid and cysteine were usually used as the starting monomers [23]. This is a valuable try to synthesize biodegradable polyesters for biomedical applications via molecular structural design to endow them with inherent photoluminescent performance.

Peer review under responsibility of KeAi Communications Co., Ltd.
* Corresponding author.
E-mail address: caiqing@mail.buct.edu.cn (Q. Cai).

https://doi.org/10.1016/j.bioactmat.2020.01.008
Received 22 October 2019; Received in revised form 13 January 2020; Accepted 14 January 2020

Inspired by this idea, we have synthesized a kind of biodegradable photoluminescent polyorganophosphazene (POPP) via nucleophilic substitution reaction by grafting an organic fluorophore onto the polyphosphazene backbone [24]. The fluorescent molecule (termed as TPCA) was derived from citric acid and 2-aminoethanethiol, and could react with polydichlorophosphazene (PDCP) easily. Amino acid ester (e.g. alanine ethyl ester) was selected as the co-substituted group, and the degradation rates of resulting POPPs could be controlled by adjusting the grafting ratios of substituted groups. In comparison with polyesters, amino acid ester substituted POPPs demonstrate remarkable advantages as scaffolding materials. The flexibility in the chemical synthesis of POPPs makes the polymers easy to be functionalized with various substituted groups, including the organic fluorophores. The degradation products of biodegradable POPPs are amine, phosphate and corresponding pendant compounds (e.g. amino acid), which are pH-buffered. They would not cause the possible problem resulting from the accumulation of acidic byproducts derived from biodegradable polyesters [25–28]. Particularly, biodegradable POPPs are proven as good scaffolding materials for bone regeneration, showing significant osteoinductivity due to their richness of phosphorus and nitrogen elements [29,30].

In this study, the biodegradable photoluminescent poly[(TPCA)(ethylalanato)phosphazene] (PTA) was synthesized following our previous study [24], and its potential in inducing bone regeneration was investigated by implanting porous scaffolds into critical-sized rat calvarial defects (φ = 8 mm). More importantly, the *in vivo* degradation of the PTA polymeric scaffold was evaluated by taking advantage of its photoluminescent performance. *In vitro* cell culture using bone marrow mesenchymal stromal cells (BMSCs) was also conducted on both PTA and PLLA scaffolds to identify the superior osteoinductivity of POPPs to conventional polyesters.

2. Materials and methods

2.1. Materials

Compounds for the synthesis of POPPs, including hexachlorocyclotriphosphazene (HCCP), alanine ethyl ester hydrochloride and glycine ethyl ester hydrochloride, were purchased from Aladdin (China). HCCP was purified by recrystallization and sublimation (50 °C, 10 mbar). 2-Aminoethanethiol was purchased from Tokyo Chemical Industry (Japan). PLLA (M_w = 100,000) was purchased from Shandong Pharmaceutical Sciences Pilot Plant (China). All other reagents and solvents used in the study were analytical grade and supplied by Beijing Chemical Reagent Co., Ltd. (China).

2.2. POPP synthesis and characterization

Two kinds of POPPs, including PTA and poly[(ethylalanato)(ethylglycinato)]phosphazene (PAGP), were synthesized according to our previous studies [24,31]. Briefly, TPCA was synthesized by the reaction of citric acid and 2-aminoethanethiol, then it reacted with PDCP in the presence of triethylamine, followed by reacting with alanine ethyl ester to obtain PTA. PAGP was obtained by reacting alanine ethyl ester and glycine ethyl ester with PDCP in sequence. The PDCP was prepared by bulk ring-opening polymerization of HCCP.

The two polymers were characterized by ^{1}H nuclear magnetic resonance (NMR, Bruker AV600) spectra and intrinsic viscosity ([η]) measurement (30 °C, in tetrahydrofuran). The PTA polymer was determined ~10 mol.% TPCA and ~90 mol.% alanine ethyl ester side groups, showing [η] ~ 50 dL/g and quantum yield ~25% [24]. The PAGP polymer was determined ~70 mol.% alanine ethyl ester and ~30 mol.% glycine ethyl ester, showing [η] ~ 90 dL/g [31].

2.3. Scaffold preparation and characterization

Thermal-induced phase separation technique was applied to prepare 3D porous scaffolds. The desired polymer (PTA, PAGP, or PLLA) was dissolved in 1, 4-dioxane to get a clear solution at the concentration of 15 wt%. Then the solution was transferred into Teflon molds and stored at −20 °C for 24 h. Subsequently, the molds were moved to a lyophilizer (−40 °C, 10 mbar) and freeze-dried for 48 h until constant weight.

Cross-sections of the prepared scaffolds were observed with scanning electron microscope (SEM, JEOLJSM-7500F, Japan) after being sputter-coated with gold. The mean pore diameter of scaffold was estimated by Nanomeasurer® software based on multiple SEM images. For compression study, disc-like scaffolds (7.8 mm in diameter, 1.5 mm in thickness) were tested on a mechanical test device (Instron 5848) at the compression rate of 2 mm/min at room temperature to an ultimate strain of 80%. To exam the photoluminescent feature of the PTA scaffold, the samples were exposed to visible light or ultraviolet light (365 nm), and photos were taken.

2.4. Cytocompatibility assay

Sprague Dawley (SD) rat BMSCs were purchased from Cyagen Bioscience (China) and cultured in α-modified eagle medium (α-MEM, Hyclone, USA) supplemented with 10% fetal bovine serum (FBS, Gibco, USA) and 1% (v/v) penicillin/streptomycin (Gibco, USA). Before cell seeding, scaffolds (7.8 mm in diameter, 1.5 mm in thickness) were exposed to ultraviolet light overnight, followed by rinsing with PBS and culture medium several times. Each scaffold was fitted into one well of 24-well plates, with BMSCs being seeded onto the scaffolds at a density of 2×10^3 cells/scaffold. BMSCs cultured on tissue culture polystyrene (TCPs) were set as the control. At pre-determined intervals (1, 3, 5 and 7 days), 10% CCK-8 (Dojindo, Japan) solution was added into the well, followed by keeping the system at 37 °C for 2 h. Then optical density (OD) values were recorded at 450 nm with a microplate reader (Bio-Rad 680, USA), which were positively related to cell numbers. For easy comparison, the OD value measured in each group at the first day was set as 1, and the OD values of other time points were all normalized to it in corresponding groups.

2.5. Osteogenic differentiation assay

The scaffolds were fitted into 24-plates and BMSCs were seeded onto each scaffold at a density of 5×10^4 cells/scaffold, using cells cultured on TCPs as the control. Twenty-four hours later, the culture medium was replaced by osteoinductive medium, which was made by adding 50 μM ascorbic acid, 10 mM β-glycerophosphate and 100 nM dexanethasone into the culture medium. The inductive culture continued for 21 days with the medium being refreshed every 2 days. At 3, 7, 14 and 21 days of the culture, the medium in each well was discarded and cell lysates for quantitative analysis were prepared. Briefly, to each well, 200 μL cell lysis buffer containing 1% Triton X-100, 200 mM Tris and 150 mM NaCl were added, then cell lysates were ready for use after freezing-thawing the systems for three times and centrifugation. Evaluations on alkaline phosphatase (ALP, Nanjing Jiancheng, China), collagen I (Col-I, BlueGene, China) and calcium deposition (Sigma, USA) were conducted by corresponding kits based on the manufacturers' protocols. The data of ALP activity and Col-I secretion were normalized to the total protein content that was determined by BCA protein assay kit (Thermofisher, USA), using bovine serum albumin (BSA) as the standard. For the cells having cultured on different scaffolds for 14 days, the cell/scaffold complexes were retrieved, rinsed with PBS, fixed with paraformaldehyde (4%, PFA, Solarbio, China) for 4 h under room temperature, and then stained with alizarin red (Solarbio, China) to visualize the calcium depositions in different cases.

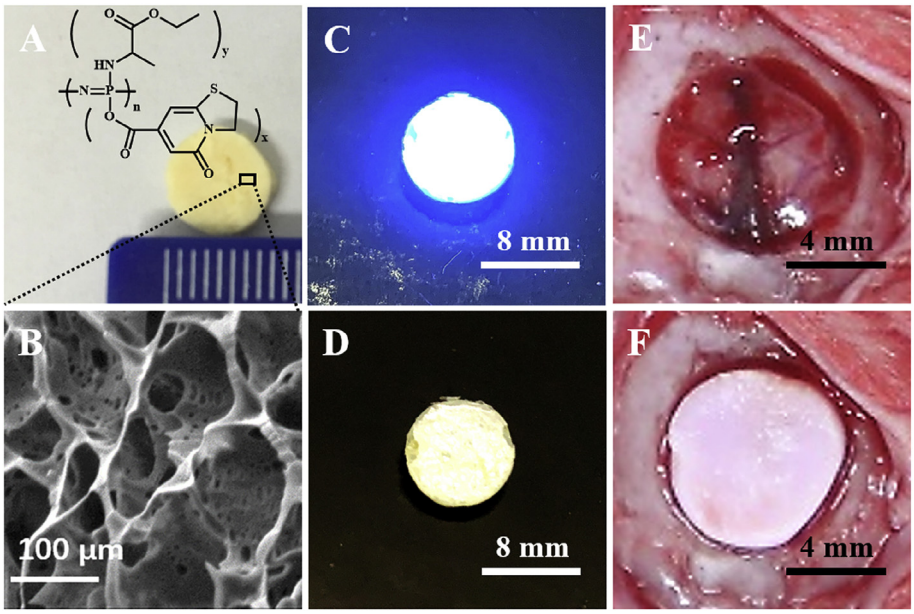

Fig. 1. (A) Gross appearance and (B) cross-section of the PTA scaffold prepared by thermal-induced phase separation technique. Photoluminescent performance evaluated by exposing the PTA scaffold to (C) ultraviolet (365 nm) and (D) visible light. (E) The created 8 mm defect in SD rat calvaria and (F) the implanted PTA scaffold.

2.6. Rat calvarial defect creation and scaffold implantation

Care and use of laboratory animals followed the protocol that was approved by the Animal Care and Use Committee of Tianjin Medical University (China) with international standards on animal welfare. Thirty-six male SD rats (5–6 weeks old, 200–250 g) were used to create the critical-sized calvarial defect (8 mm in diameter) for bone regeneration study. The rats were randomly divided into 3 groups and treated as follows: 1) defects filled with PTA scaffolds (PTA group); 2) defects filled with BMSCs pre-loaded PTA scaffolds (PTA-BMSC group); 3) defects left unfilled (control group). Briefly, rats were anesthesized with chloral hydrate (0.5 mL/250 g). After shaving, the 8 mm circular defects were drilled at the central region of the calvaria with a trephine bur. The periosteum was completely removed while the underlying dura mater was kept intact according to an established protocol [32]. After corresponding scaffolds (7.8 mm in diameter, 1.5 mm in thickness) were filled into the defects, the overlying tissue was closed with surgical staples. The PTA scaffolds with pre-loaded BMSCs were prepared by seeding the cells at a density of 1×10^5 cells/scaffold, and *in vitro* cultured for 3 days before the implantation. After surgery, all rats were allowed to move with food and water *ad libitum*. At 4, 8 and 16 weeks post-surgery, 4 rats were sacrificed for each group. The retrieved skulls were fixed 48 h in neutral buffered formalin (10%) for further analysis.

2.7. Bone regeneration evaluation

The harvested skulls were examined with micro-CT (Skyscan 1176, Bruker, Belgium). The 1.6 version of NR econ® software was used for 3D reconstruction and image viewing. An 8 mm diameter circular region was selected in the center of calvarial defect area to perpendicularly locate the cylindrical volume of interest for analysis. New bone volume fraction (BV/TV) and bone mineral density (BMD) were obtained using CT AN software version 1.14 (Bruker micro-CT, Kontich, Belgium).

For histological analysis, sections in 5 μm thickness were cut after skulls were decalcified in a rapid decalcifier (RapidCal, Immuno, ZS-Bio, China) for 48 h under room temperature, dehydrated by 70% ethanol and embedded in paraffin. Hematoxylin-eosin (H&E, Senbeijia, China) and Masson's trichrome (Senbeijia, China) staining were performed separately, and images were captured with digital slice scanning equipment (Nanozoomer, Hamamatsu, Japan).

2.8. Visualizing the in vivo degradation of PTA scaffold

At 4, 8 and 16 weeks post-surgery, one skull retrieved from the PTA group was embedded directly in photocured acrylate resin without decalcification. Sections in 5 μm thickness were prepared and the sections were observed by confocal laser scanning microscope (CLSM, TCS SP8, Leica) to illustrate the *in vivo* degradation of the implanted PTA scaffold. The fluorescent intensities were estimated by an image pro plus® (IPP) software. Briefly, four square regions (1×1 cm^2) were randomly selected on each skull section, and the fluorescent intensity of each sample was averaged from the assessed values of the four random areas following the IPP software specification. Meanwhile, these sections were also observed by optical microscope.

2.9. Statistical analysis

All quantitative data was represented as mean ± SD (standard deviation) for $n \geq 3$. Statistical analysis was carried out by one way analysis of variance (ANOVA) with Turkey's test. Differences between groups of $^*p < 0.05$ were considered statistically significant, $^{**}p < 0.01$ were considered highly significant.

3. Results

3.1. The PTA scaffold prepared for in vivo implantation

PTA was dissolved in 1,4-dioxane and PTA scaffold was prepared by the thermal-induced phase separation technique (Fig. 1A). From Fig. 1B, the interconnected porous structure of the scaffold was clearly presented. The mean pore diameter was estimated approximate 110 μm. The PTA is a photoluminescent polymer, therefore, the PTA scaffold displayed strong fluorescence when it was exposed to ultraviolet light, emitting intense blue fluorescence (Fig. 1C). No such phenomenon could be observed when the scaffold was exposed to visible light (Fig. 1D). The photos shown in Fig. 1E, F revealed the success in creating the rat calvarial defect model and the perfect fitting of the PTA scaffold in site.

PAGP and PLLA scaffolds were prepared similarly for comparison, and their porous structures were similar to that of PTA scaffold under SEM observation (images not shown). The three kinds of scaffolds were submitted to compression test and the obtained stress-strain curves are presented in Fig. 2. It was identified that the PLLA scaffold displayed

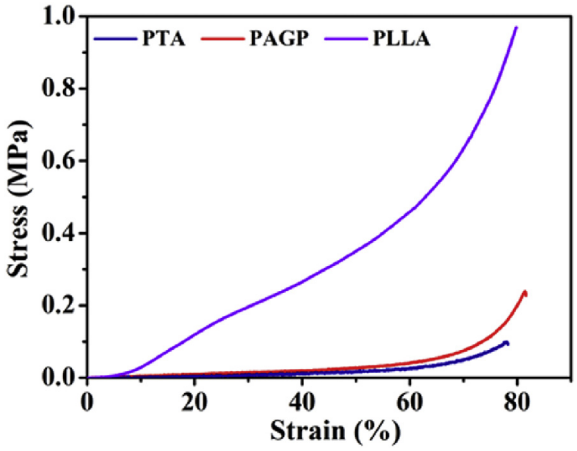

Fig. 2. Stress-strain curves obtained for PTA, PAGP and PLLA scaffolds via compression test.

much stronger compression strength than both the POPP (PTA and PAGP) scaffolds. It was suggested that the semi-crystalline feature of PLLA and the flexible polyphosphazene backbone caused the difference. The PTA and PAGP scaffolds shared comparable compression performance due to the similarity in their chemical structures.

3.2. PTA scaffold favoring cell proliferation and differentiation in vitro

PTA, PAGP and PLLA all were determined non-cytotoxic for cell seeding and proliferation. As shown in Fig. 3A, the BMSCs seeded on different scaffolds proliferated continuously from 1 day to 7 days. The cells on PLLA scaffolds shared similar growth rate with those cells on the TCPs control, and the two POPP scaffolds displayed similar cell growth rates. It was noted that both the PTA and the PAGP scaffolds could significantly promote the proliferation of BMSCs in comparison with the PLLA scaffolds. The results of osteogenic differentiation revealed a similar trend for cells cultured on the three kinds of scaffolds and the TCPs control. The highest expression levels of the osteogenic markers, i.e., the ALP expression, the Col-I secretion and the Ca deposition, were found in the two POPP groups, followed by the PLLA group and the control group, showing significant difference between the former and the latter cases (Fig. 3B-D). The images of alizarin red staining apparently confirmed the previous findings (Fig. 3E). It could be seen that the BMSCs cultured on both the PTA and the PAGP scaffolds displayed much deeper red color than those on the PLLA scaffold, revealing the significant formation of calcium nodules on the two POPP scaffolds. These *in vitro* results confirmed that PTA and PAGP scaffolds were superior in inducing osteogenic differentiation of BMSCs in comparison with the polyester-type scaffold. At meantime, the photoluminescent PTA scaffold could regulate cell activities in a similar way to the PAGP scaffold, which suggested the introduction of the fluorescent TPCA side group did not cause adverse effect. Therefore, the PTA scaffolds were expected to promote osteogenesis by implanting them into the rat calvarial defects.

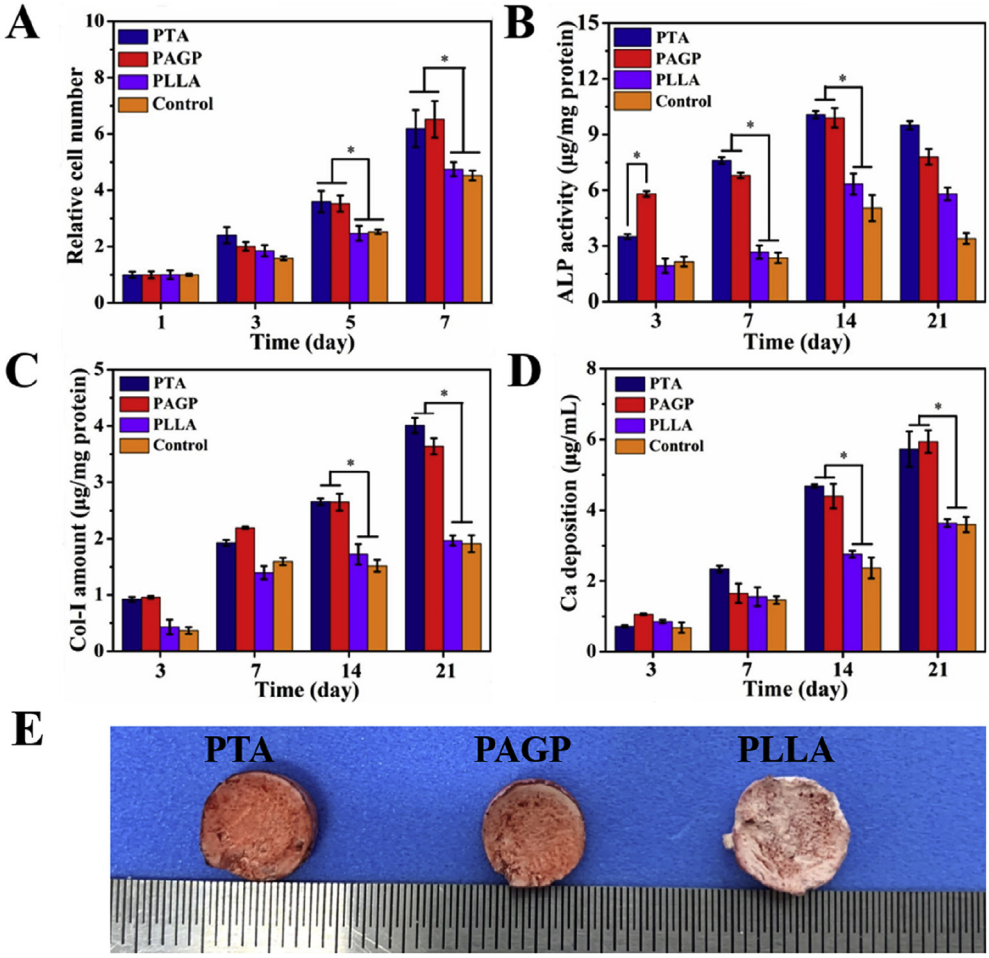

Fig. 3. Evaluating the cytocompatibility and osteogenic differentiation capacity of different scaffolds by: (A) BMSCs proliferation on scaffolds; (B) ALP expression; (C) Col-I secretion; (D) Ca deposition; (E) alizarin red staining. Error bars represent mean ± SD for n = 4, *p < 0.05 (significant).

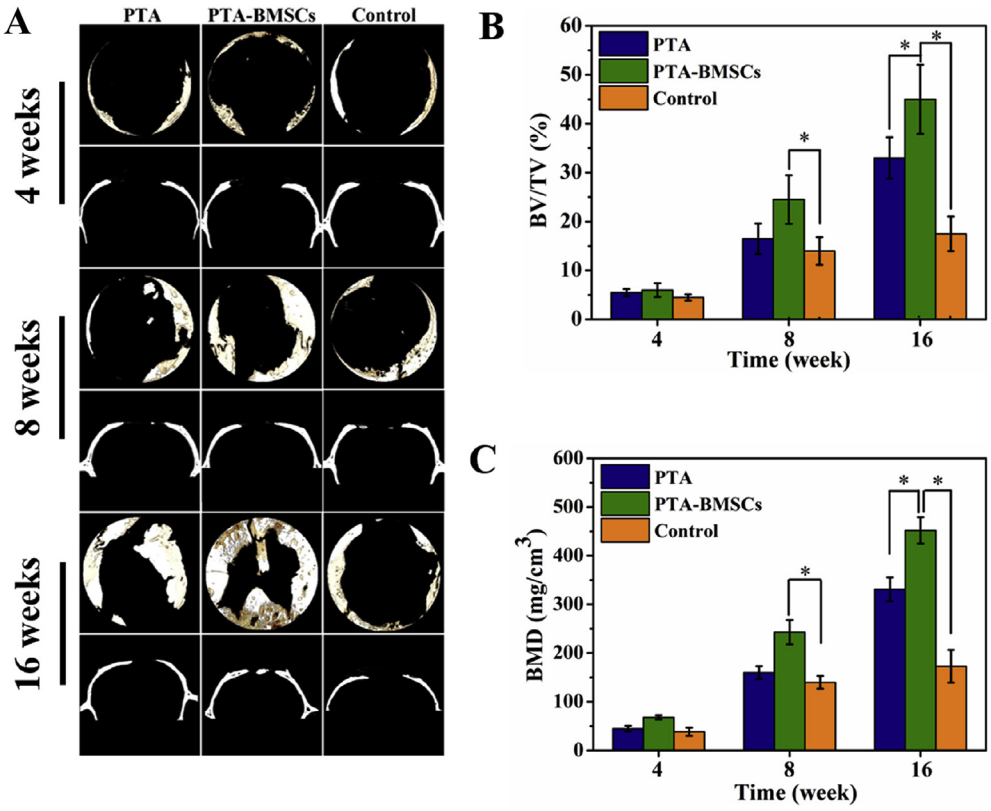

Fig. 4. Evaluating the bone regeneration capacity induced by PTA scaffolds with or without pre-seeded BMSCs by micro-CT analysis: (A) Reconstructed 3D micro-CT images of rat calvaria at 4, 8 and 16 weeks post-surgery; (B) BV/TV and (C) BMD values estimated quantitatively from corresponding reconstructed micro-CT images. Error bars represent mean ± SD for n = 4, *p < 0.05 (significant) and **p < 0.01 (highly significant).

3.3. PTA scaffold favoring bone regeneration in vivo

To regenerate the rat calvarial defect, PTA scaffolds were implanted with or without BMSCs being pre-seeded. The bone regeneration efficiency was evaluated by micro-CT analysis and histological staining. From the reconstructed micro-CT images (Fig. 4A), it was observed that new bone barely formed in the control group even at 16 weeks post-surgery, indicating the critical-sized bone defect was hard to be self-repaired. On the contrary, distinguishable new bone formation could be detected for the defects filled with the PTA or the PTA-BMSCs scaffolds. At 16 weeks post-surgery, the group with implanted BMSCs demonstrated the most effective osteogenesis. Confirmed by the quantitative analysis on BV/TV and BMD values, as shown in Fig. 4B, C, the values reached 45.1 + 7.1% and 462.4 + 27.1 mg/cm^3, respectively, in the PTA-BMSCs group, followed by the 33.4 + 4.2% and 353.5 + 24.2 mg/cm^3 of the PTA group, and both them displayed significantly higher levels than those in the control group.

From the H&E stained images shown in Fig. 5, both the PTA and the PTA-BMSCs scaffolds displayed excellent biocompatibility with no hint of inflammation. In combining those Masson's trichrome stained images shown in Fig. 6, it was determined that the defect area in the control group was mainly filled with fibrous connective tissues. The defects filled with PTA or PTA-BMSCs were seen rich collagen components and obvious new bone formation. Particularly, the involvement of BMSCs could promote osteogenesis more significantly, further indicating the implanted PTA scaffold being non-cytotoxic, favoring cell proliferation and differentiation, which led to faster new bone formation.

3.4. The in vivo degradation of PTA scaffold visualized via fluorescence

Without decalcification, slices were cut from the retrieved skulls from both the PTA and the PTA-BMSCs groups, and submitted to observation under CLSM (Fig. 7). At 4 weeks post-implantation, the PTA scaffolds still displayed strong blue fluorescence when the slices were excited by ultraviolet light (365 nm), and porous structure was clearly

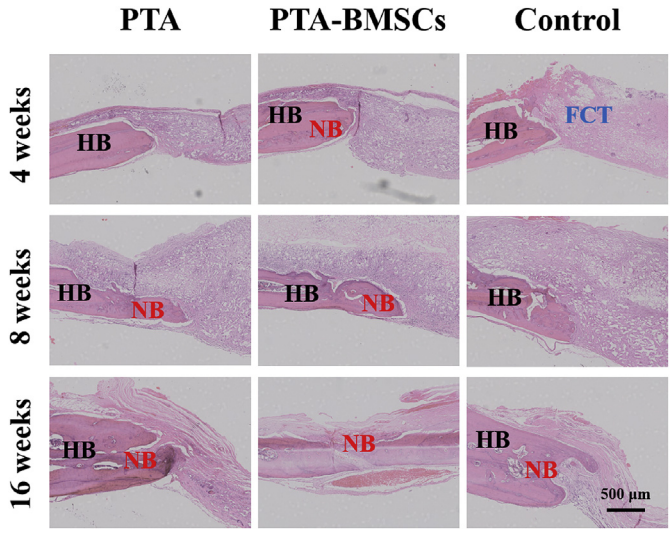

Fig. 5. H&E analysis to evaluate the new bone formation in defects being differently treated at 4, 8 and 16 weeks post surgery. NB indicates newly formed bone, HB indicates host bone and FCT indicates fibrous connective tissues.

seen. At 8 weeks post-implantation, the fluorescent intensities of the scaffolds faded and the porous structure became indistinct. Until the 16 weeks post-implantation, the fluorescence of the PTA scaffold almost could not be detected. Basing on these images, the fluorescent intensities of the residual PTA scaffolds were quantified using a IPP software and plotted as Fig. 8. From the figure, the gradual decreases in fluorescent intensities were identified for both the PTA and the PTA-BMSCs cases from 4 to 16 weeks post-implantation. These changes observed in the fluorescent intensities of the photoluminescent PTA scaffolds clearly illustrated their *in vivo* degradation alongside longer implantation time, and the presence of BMSCs or not barely influenced their degradation rates. From the images taken under optical

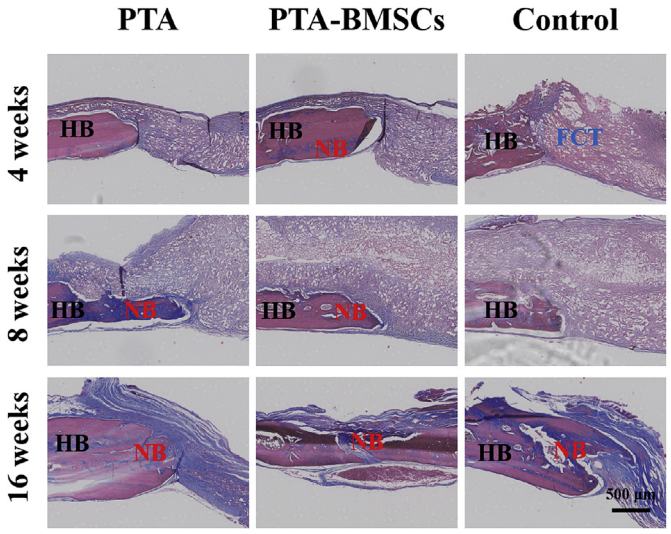

Fig. 6. Masson's trichrome staining analysis to evaluate the new bone formation in defects being differently treated at 4, 8 and 16 weeks post surgery. NB indicates newly formed bone, HB indicates host bone and FCT indicates fibrous connective tissues.

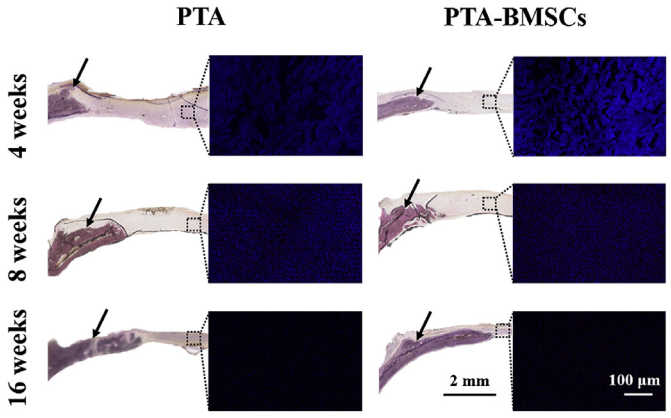

Fig. 7. The *in vivo* degradation of PTA scaffold visualized via its photoluminescent feature with the aid of CLSM on skull slices retrieved from both the PTA and the PTA-BMSCs groups (arrows indicating the edge of the defect region).

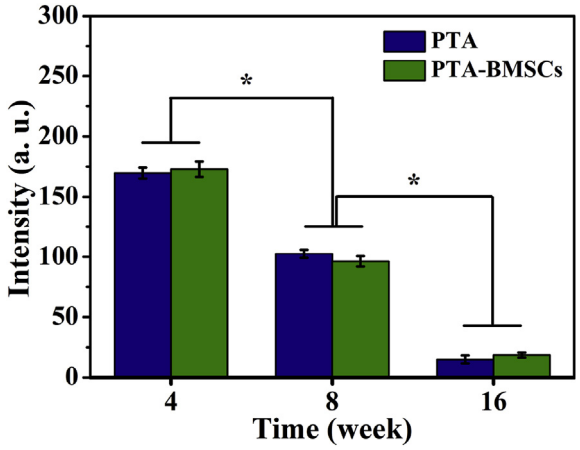

Fig. 8. Quantitative analysis on the fluorescent intensities of PTA scaffolds gradually decreasing along with longer implantation time to reflect their *in vivo* degradation. Error bars represent mean ± SD for n = 4, *p < 0.05 (significant).

microscope, it was not possible to judge the degradation of the implanted materials, while new bone formation sprouting from the defect edge could be identified alongside the scaffold degradation. As time went on, the newly formed bone tissue extended into the defect center, and the pre-seeded BMSCs could accelerate this procedure remarkably.

4. Discussion

To regenerate injured tissue *in vivo*, a key operation is the implantation of a scaffold with a proper biodegradation behavior, which provides support and space for cell locating, proliferating and differentiating into the newly formed tissue [33]. Thus, it is quite attractive if the degradation of the implanted scaffold can be visualized *in-situ*. Conventional lactone-based homopolymers and copolymers like PLA, PCL and PLGA are invisible *in-situ* via the bio-imaging mechanisms such as AIE, PA, MRI and/or PLE, because these polymers lack functional groups. And they are hard to be endowed with the photoluminescent capacity by incorporating fluorescent groups for their chemical structures [34,35]. To avoid the use of imaging materials with potential cytotoxicity, e.g. the Qdots, biodegradable scaffolding materials with intrinsic photoluminescent feature for *in vivo* applications were strongly proposed [30]. Promisingly, it was reported that the reaction product (e.g. TPCA) from citric acid and compounds containing the cysteamine structure could generate strong fluorescence as being excited by ultraviolet light [24,36]. Researchers had taken advantage of this feature in synthesizing degradable photoluminescent polyesters via condensation polymerization for biomedical applications [37]. And in our lab, a kind of degradable photoluminescent POPP was also developed by grafting the TPCA fluorophore onto the polyphosphazene backbone, i.e., the PTA polymer in the present study, which used the alanine ethyl ester as the co-substitution side group and its quantum yield was estimated ~25% [24]. The porous scaffold made of the PTA polymer displayed strong fluorescence under ultraviolet light, while not under the visible light (Fig. 1).

The PTA polymer was designed to target bone regeneration, due to the well-known facts that amino acid ester substituted POPPs are biocompatible and degradable, as well as, osteocompatible, benefiting from their richness in phosphorus element, which is pivotal in osteogenesis [38,39]. By implanting the PTA scaffolds into the calvarial defects created in rat model for 4, 8 and 16 weeks, the skulls were retrieved for CLSM examination. As shown in Fig. 7, the presence of the scaffolds could be clearly illustrated when being excited with ultraviolet light. The changes in scaffold morphology and fluorescent intensity were distinguishable alongside the longer implantation time, indicating the *in vivo* degradation of the scaffold. It was noted that the fluorescence of the PTA polymer was quite stable during the implantation, without significant fluorescence quenching phenomenon. The fluorescence of small molecular fluorophores are likely to be quenched, due to their high mobility and molecular collision [40]. It was different in the PTA case, in which, the fluorophore was grafted as the side group onto the polyphosphazene backbone, and the alternate -P═N- unit in the backbone did not form a conjugated structure [26]. Thus, the collision between TPCA side groups was inhibited and the electron transportation along the backbone was also inhibited, which resulted in the excellent photoluminescent feature of the PTA polymer [24]. This advantage made the PTA scaffold to be a competitive candidate for *in vivo* application, particularly, for bone tissue engineering.

The non-cytotoxicity and the osteocompatibility of the PTA scaffold was confirmed by *in vitro* culture using BMSCs via cell proliferation and osteogenic differentiation, demonstrating superiority over the conventional PLLA scaffold (Fig. 3). These findings were in accordance with other reports on biodegradable POPPs (e.g. PAGP) for biomedical applications [31]. In literature, *in vivo* evaluations on biodegradable POPPs to regenerate bone tissue were not so common [27]. One possible reason for this phenomenon might be the weaker mechanical property of POPPs in comparison with polyesters, as being reflected by

Fig. 2. In this study, though the PTA scaffold presented lower mechanical strength than the PLLA, the *in vivo* evaluations revealed that the PTA scaffold was robust enough to perform the implantation (Fig. 1F), and its porous structure could maintain for a long time during the implantation (Fig. 7). Therefore, cells had migrated into the scaffold to form new bone tissue sprouting from the defect edge in the PTA group (Figs. 4–6). If BMSCs were pre-loaded onto the PTA scaffold as seed cells, the osteogenesis could be further remarkably promoted in the PTA-BMSCs group, showing the highest BV/TV and BMD values among all the groups (Fig. 4B, C). Alongside the degradation of PTA scaffolds in both the groups, more newly formed bone tissues had been identified at a longer time post-implantation. On the contrary, the unfilled control group displayed inferior bone regeneration and fibrous connective tissue ingrowth (Figs. 5–6).

With all these findings and discussions, it was suggested that biodegradable photoluminescent POPPs (e.g. the PTA polymer) demonstrated strong potentials as scaffolding materials for their capacities of *in-situ* bio-imaging, cyto- and tissue-compatibility. They could be implanted directly to induce bone regeneration, or be implanted applying the traditional tissue engineering strategy that cells like BMSCs were pre-seeded to accelerate the osteogenesis [41,42].

5. Conclusions

Benefiting from the flexibility of the phosphazene chemistry, it is readily to design and to synthesize POPPs with desirable performances. Targeting tissue engineering, biodegradable POPPs were able to be modified with fluorophore side groups (e.g. the TPCA) to endow the polymers with photoluminescent performance, which highlighted them (e.g. the PTA) as scaffolding materials. The photoluminescent performance would be a great help to evaluate the *in-situ* degradation of implanted scaffolds via the fluorescent bio-imaging system. Due to their richness of phosphorus and nitrogen elements, particularly, biodegradable photoluminescent POPPs are expected to promote effective and efficient bone regeneration as proved in the present study, showing promising future in bone tissue engineering.

Declaration of competing interestCOI

The authors declare no conflict of interest.

CRediT authorship contribution statement

Yiqian Huang: Investigation, Validation, Writing - original draft. **Zhaohui Huang:** Conceptualization, Investigation. **Huanhuan Liu:** Validation. **Xu Zhang:** Formal analysis. **Qing Cai:** Conceptualization, Methodology, Writing - review & editing. **Xiaoping Yang:** Supervision.

Acknowledgements

The authors acknowledged the financial support from National Key R&D Program of China (2017YFC1104302/4300), National Natural Science Foundation of China (51873013, 81871761).

References

[1] R.J. Mondschein, A. Kanitkar, C.B. Williams, S.S. Verbridge, T.E. Long, Polymer structure-property requirements for stereolithographic 3D printing of soft tissue engineering scaffolds, Biomaterials 140 (2017) 170–188, https://doi.org/10.1016/j.biomaterials.2017.06.005.

[2] L.G. Bracaglia, B.T. Smith, E. Watson, N. Arumugasaamy, A.G. Mikos, J.P. Fisher, 3D printing for the design and fabrication of polymer-based gradient scaffolds, Acta Biomater. 56 (2017) 3–13, https://doi.org/10.1016/j.actbio.2017.03.030.

[3] L. Zhang, G. Yang, B.N. Johnson, X. Jia, Three-dimensional (3D) printed scaffold and material selection for bone repair, Acta Biomater. 84 (2019) 16–33, https://doi.org/10.1016/j.actbio.2018.11.039.

[4] J.Z. Yu, E. Korkmaz, M.I. Berg, P.R. LeDuc, O.B. Ozdoganlar, Biomimetic scaffolds with three-dimensional undulated microtopographies, Biomaterials 128 (2017) 109–120, https://doi.org/10.1016/j.biomaterials.2017.02.014.

[5] A. Ferrández-Montero, M. Lieblich, J.L. González-Carrasco, R. Benavente, V. Lorenzo, R. Detsch, A.R. Boccaccini, B. Ferrari, Development of biocompatible and fully bioabsorbable PLA/Mg films for tissue regeneration applications, Acta Biomater. (2019), https://doi.org/10.1016/j.actbio.2019.05.026.

[6] H. Cao, N. Kuboyama, A biodegradable porous composite scaffold of PGA/β-TCP for bone tissue engineering, Bone 46 (2010) 386–395, https://doi.org/10.1016/j.bone.2009.09.031.

[7] J.R. Thompson, K.S. Worthington, B.J. Green, N.K. Mullin, C. Jiao, E.E. Kaalberg, L.A. Wiley, I.C. Han, S.R. Russell, E.H. Sohn, C.A. Guymon, R.F. Mullins, E.M. Stone, B.A. Tucker, Two-photon polymerized poly(caprolactone) retinal cell delivery scaffolds and their systemic and retinal biocompatibility, Acta Biomater. 94 (2019) 204–218, https://doi.org/10.1016/j.actbio.2019.04.057.

[8] Y. Lai, Y. Li, H. Cao, J. Long, X. Wang, L. Li, C. Li, Q. Jia, B. Teng, T. Tang, J. Peng, D. Eglin, M. Alini, D.W. Grijpma, G. Richards, L. Qin, Osteogenic magnesium incorporated into PLGA/TCP porous scaffold by 3D printing for repairing challenging bone defect, Biomaterials 197 (2019) 207–219, https://doi.org/10.1016/j.biomaterials.2019.01.013.

[9] L. Wang, B. Li, F. Xu, Y. Li, Z. Xu, D. Wei, Y. Feng, Y. Wang, D. Jia, Y. Zhou, Visual *in vivo* degradation of injectable hydrogel by real-time and non-invasive tracking using carbon nanodots as fluorescent indicator, Biomaterials 145 (2017) 192–206, https://doi.org/10.1016/j.biomaterials.2017.08.039.

[10] D. Yang, J. Xiao, B. Wang, L. Li, X. Kong, J. Liao, The immune reaction and degradation fate of scaffold in cartilage/bone tissue engineering, Mater. Sci. Eng. C 104 (2019), https://doi.org/10.1016/j.msec.2019.109927.

[11] Y. Wang, Y. Zhang, J. Wang, X.J. Liang, Aggregation-induced emission (AIE) fluorophores as imaging tools to trace the biological fate of nano-based drug delivery systems, Adv. Drug Deliv. Rev. 143 (2019) 161–176, https://doi.org/10.1016/j.addr.2018.12.004.

[12] H. Huang, M. Liu, S. Luo, K. Wang, Q. Wan, F. Deng, D. Xu, X. Zhang, Y. Wei, One-step preparation of AIE-active dextran via formation of phenyl borate and their bioimaging application, Chem. Eng. J. 304 (2016) 149–155, https://doi.org/10.1016/j.cej.2016.06.001.

[13] J. Lia, R. Jiang, Q. Wang, X. Li, X. Hu, Y. Yuan, X. Lu, W. Wang, W. Huang, Q. Fan, Semiconducting polymer nanotheranostics for NIR-II/photoacoustic imaging-guided photothermal initiated nitric oxide/photothermal therapy, Biomaterials 217 (2019) 119304, , https://doi.org/10.1016/j.biomaterials.2019.119304.

[14] P. Li, Z. He, C. Luo, Y. Xiao, Y. Wang, J. Hu, G. Li, H. Jiang, W. Zhang, α-Fe_2O_3@dopamine core-shell nanocomposites and their highly enhanced photoacoustic performance, Appl. Surf. Sci. 466 (2019) 185–192, https://doi.org/10.1016/j.apsusc.2018.10.021.

[15] N. Torkashvand, N. Sarlak, Polymerized graphene oxide/$MnCe_{0.5}Fe_{1.5}O_4$ nanoferrofluid as a T_2- and T_2*-weighted contrast agent for magnetic resonance imaging, Colloids Surf., B 185 (2019), https://doi.org/10.1016/j.colsurfb.2019.110555.

[16] M. Zhang, T. Zheng, B. Sheng, F. Wu, Q. Zhang, W. Wang, J. Shen, N. Zhou, Y. Sun, Mn^{2+} complex-modified polydopamine- and dual emissive carbon dots based nanoparticles for *in vitro* and *in vivo* trimodality fluorescent, photothermal, and magnetic resonance imaging, Chem. Eng. J. 373 (2019) 1054–1063, https://doi.org/10.1016/j.cej.2019.05.107.

[17] F.F. Chen, Y.J. Zhu, Y.G. Zhang, R.L. Yang, H.P. Yu, D.D. Qin, Z.C. Xiong, Portable and writable photoluminescent chalk for on-site information protection on arbitrary substrates, Chem. Eng. J. 369 (2019) 766–774, https://doi.org/10.1016/j.cej.2019.03.153.

[18] H. Niu, X. Li, H. Li, Z. Fan, J. Ma, J. Guan, Thermosensitive, fast gelling, photoluminescent, highly flexible, and degradable hydrogels for stem cell delivery, Acta Biomater. 83 (2019) 96–108, https://doi.org/10.1016/j.actbio.2018.10.038.

[19] J. Yang, Y. Zhang, S. Gautam, L. Liu, J. Dey, W. Chen, R.P. Mason, C.A. Serranoe, K.A. Schug, L. Tang, Development of aliphatic biodegradable photoluminescent polymers, Proc. Natl. Acad. Sci. 106 (2009) 10086–10091, https://doi.org/10.1073/pnas.0906215106.

[20] F. Pinaud, X. Michalet, L.A. Bentolila, J.M. Tsay, S. Doose, J.J. Li, G. Iyer, S. Weiss, Advances in fluorescence imaging with quantum dot bio-probes, Biomaterials 27 (2006) 1679–1687, https://doi.org/10.1016/j.biomaterials.2005.11.018.

[21] K.M. Dupont, K. Sharma, H.Y. Stevens, J.D. Boerckel, A.J. Garcíaa, R.E. Guldberg, Human stem cell delivery for treatment of large segmental bone defects, Proc. Natl. Acad. Sci. 107 (2010) 3305–3310, https://doi.org/10.1073/pnas.0905444107.

[22] S. Duan, S. Ma, Z. Huang, X. Zhang, X. Yang, P. Gao, M. Yin, Q. Cai, Visualization of *in vivo* degradation of aliphatic polyesters by a fluorescent dendritic star macromolecule, Biomed. Mater. 10 (2015) 065003, , https://doi.org/10.1088/1748-6041/10/6/065003.

[23] Z. Xie, J.P. Kim, Q. Cai, Y. Zhang, J. Guo, R.S. Dhami, L. Li, B. Kong, Y. Su, K.A. Schug, J. Yang, Synthesis and characterization of citrate-based fluorescent small molecules and biodegradable polymers, Acta Biomater. 50 (2017) 361–369, https://doi.org/10.1016/j.actbio.2017.01.019.

[24] Z. Huang, L. Yang, X. Zhang, B. Ruan, X. Hu, X. Deng, Q. Cai, X. Yang, Synthesis and fluorescent property of biodegradable polyphosphazene targeting long-term *in vivo* tracking, Macromolecules 49 (2016) 8508–8519, https://doi.org/10.1021/acs.macromol.6b01976.

[25] H.R. Allcock, Recent advances in phosphazene (phosphonitrilic) chemistry, Chem. Rev. 72 (1972) 315–356, https://doi.org/10.1021/cr60278a002.

[26] S. Rothemund, I. Teasdale, Preparation of polyphosphazenes: a tutorial review, Chem. Soc. Rev. 45 (2016) 5200–5215, https://doi.org/10.1039/c6cs00340k.

[27] M. Deng, S.G. Kumbar, L.S. Nair, A.L. Weikel, H.R. Allcock, C.T. Laurencin, Biomimetic structures: biological implications of dipeptide-substituted polyphosphazene–polyester blend nanofiber matrices for load-bearing bone regeneration, Adv. Funct. Mater. 21 (2011) 2641–2651, https://doi.org/10.1002/adfm.

201100275.
[28] M. Deng, L.S. Nair, S.P. Nukavarapu, T. Jiang, W.A. Kanner, X. Li, S.G. Kumbar, A.L. Weikel, N.R. Krogman, H.R. Allcock, C.T. Laurencin, Dipeptide-based polyphosphazene and polyester blends for bone tissue engineering, Biomaterials 31 (2010) 4898–4908, https://doi.org/10.1016/j.biomaterials.2010.02.058.
[29] Z. Huang, L. Yang, X. Hu, Y. Huang, Q. Cai, Y. Ao, X. Yang, Molecular mechanism study on effect of biodegradable amino acid ester–substituted polyphosphazenes in stimulating osteogenic differentiation, Macromol. Biosci. 19 (2019) 1800464, , https://doi.org/10.1002/mabi.201800464.
[30] Z.H. Huang, P.F. Wei, L. Jin, X.Q. Hu, Q. Cai, X.P. Yang, Photoluminescent polyphosphazene nanoparticles for *in situ* simvastatin delivery for improving the osteocompatibility of BMSCs, J. Mater. Chem. B. 5 (2017) 9300–9311, https://doi.org/10.1039/c7tb02281f.
[31] S. Duan, X. Yang, J. Mao, B. Qi, Q. Cai, H. Shen, F. Yang, X. Deng, S. Wang, Osteocompatibility evaluation of poly(glycine ethyl ester-co-alanine ethyl ester) phosphazene with honeycomb-patterned surface topography, J. Biomed. Mater. Res. A 101 (2013) 307–317, https://doi.org/10.1002/jbm.a.34282.
[32] P.P. Spicer, J.D. Kretlow, S. Young, J.A. Jansen, F.K. Kasper, A.G. Mikos, Evaluation of bone regeneration using the rat critical size calvarial defect, Nat. Protoc. 7 (2012) 1918–1929, https://doi.org/10.1038/nprot.2012.113.
[33] K.M. Kennedy, A. Bhaw-Luximon, D. Jhurry, Cell-matrix mechanical interaction in electrospun polymeric scaffolds for tissue engineering: implications for scaffold design and performance, Acta Biomater. 50 (2017) 41–55, https://doi.org/10.1016/j.actbio.2016.12.034.
[34] D.A. Tomalia, B. Klajnert-Maculewicz, Kayla A.M. Johnson, H.F. Brinkman, A. Janaszewska, D.M. Hedstrand, Non-traditional intrinsic luminescence: inexplicable blue fluorescence observed for dendrimers, macromolecules and small molecular structures lacking traditional/conventional luminophores, Prog. Polym. Sci. 90 (2019) 35–117, https://doi.org/10.1016/j.progpolymsci.2018.09.004.
[35] H. Tian, Z. Tang, X. Zhuang, X. Chen, X. Jing, Biodegradable synthetic polymers: preparation, functionalization and biomedical application, Prog. Polym. Sci. 37 (2012) 237–280, https://doi.org/10.1016/j.progpolymsci.2011.06.004.
[36] M. Hori, T. Kometani, H. Ueno, H. Morimoto, A new fluorometric analysis of citric acid, Biochem. Med. 11 (1974) 49–59, https://doi.org/10.1016/0006-2944(74)90094-5.
[37] D. Shan, S.R. Kothapalli, D.J. Ravnic, E. Gerhard, J.P. Kim, J. Guo, C. Ma, J. Guo, L. Gui, L. Sun, D. Lu, J. Yang, Development of citrate-based dual-imaging enabled biodegradable electroactive polymers, Adv. Funct. Mater. 28 (2018) 1801787, , https://doi.org/10.1002/adfm.201801787.
[38] Y. Wang, X. Hu, L. Zhang, C. Zhu, J. Wang, Y. Li, Y. Wang, C. Wang, Y. Zhang, Q. Yuan, Bioinspired extracellular vesicles embedded with black phosphorus for molecular recognition-guided biomineralization, Nat. Commun. 10 (2019) 2829, https://doi.org/10.1038/s41467-019-10761-5.
[39] L. Tong, Q. Liao, Y. Zhao, H. Huang, A. Gao, W. Zhang, X. Gao, W. Wei, M. Guan, P.K. Chu, H. Wang, Near-infrared light control of bone regeneration with biodegradable photothermal osteoimplant, Biomaterials 193 (2019) 1–11, https://doi.org/10.1016/j.biomaterials.2018.12.008.
[40] D. Ding, K. Li, B. Liu, B. Tang, Bioprobes based on AIE fluorogens, Accounts Chem. Res. 46 (2013) 2441–2453, https://doi.org/10.1021/ar3003464.
[41] H. Liu, H. Peng, Y. Wu, C. Zhang, Y. Cai, G. Xu, Q. Li, X. Chen, J. Ji, Y. Zhang, H. OuYang, The promotion of bone regeneration by nanofibrous hydroxyapatite/chitosan scaffolds by effects on integrin-BMP/Smad signaling pathway in BMSCs, Biomaterials 34 (2013) 4404–4417, https://doi.org/10.1016/j.biomaterials.2013.02.048.
[42] Y. Zhu, L. Kong, F. Farhadi, W. Xia, J. Chang, Y. He, H. Li, An injectable continuous stratified structurally and functionally biomimetic construct for enhancing osteochondral regeneration, Biomaterials 192 (2019) 149–158, https://doi.org/10.1016/j.biomaterials.2018.11.017.